SOLID STATE HYDROGEN STORAGE
Decoding the path through ML

1 ML model

M-H

Experimental DB

Feature Engineering

Extra-tree regressor

H2 Wt%

ΔH

2 Model evaluation and interpretation

MAE

H2 Wt% 0.31 wt%

ΔH 5.76 kJ/molH2

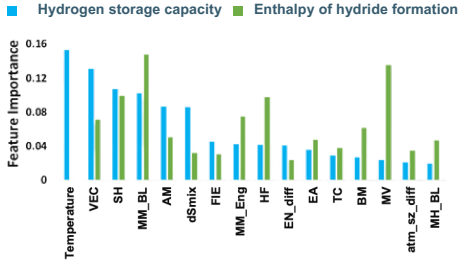

3 Predictions

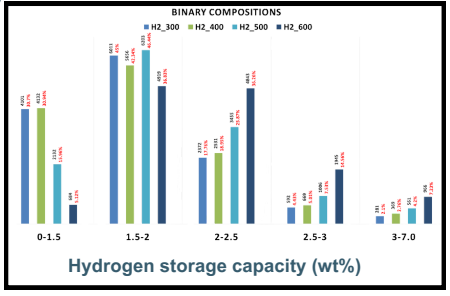

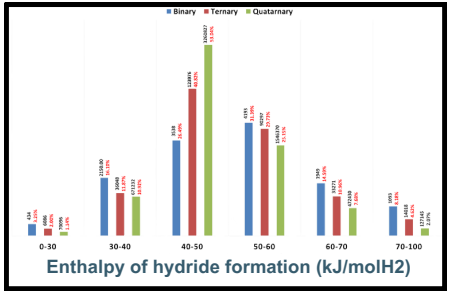

4 Trends

Scanned Compositions : 6.4 million

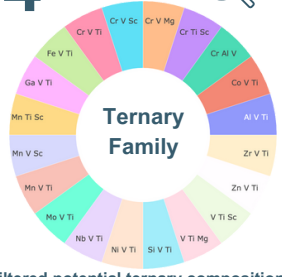

Filtered potential ternary compositions

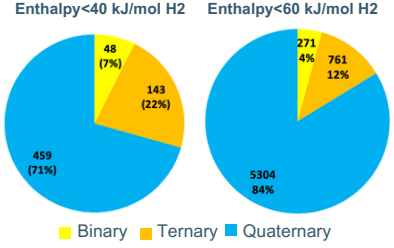

Number of composition with lower enthalpy increases with number of elements in the alloy (H2wt% >2.5 wt%)

Solid state hydrogen storage: Decoding the path through machine learning

Ashwini Verma[a,b], Nikhil Wilson[a], Kavita Joshi*[a,b]

[a] *Physical and Materials Chemistry Division, CSIR-National Chemical Laboratory, Dr. Homi Bhabha Road, Pashan, Pune-411008, India.*
[b] *Academy of Scientific and Innovative Research (AcSIR),Ghaziabad- 201002, India.*

Abstract

We present a machine learning (ML) framework HEART (**H**ydrog**E**n stor**A**ge prope**R**ty predic**T**or) for identifying suitable families of metal alloys for hydrogen storage under ambient conditions. Our framework includes two ML models that predict the **hy**drogen **s**torage capaci**t**y (HYST) and the en**th**alpy of hydride f**or**mation (THOR) of multi-component metal alloys. We demonstrate that a chemically diverse set of features effectively describes the hydrogen storage properties of the alloys. In HYST, we use absorption temperature as a feature which improved H2wt% prediction significantly. For out-of-the-bag samples, HYST predicted H2wt% with R2 score of 0.81 and mean absolute error (MAE) of 0.45 wt% whereas R2 score is 0.89 and MAE is 4.53 kJ/molH2 for THOR. These models are further employed to predict H2wt% and ΔH for $\sim$ 6.4 million multi-component metal alloys. We have identified 6480 compositions with superior storage properties (H2wt% $>$ 2.5 at room temperature and ΔH $<$ 60 kJ/molH2). We have also discussed in detail the interesting trends picked up by these models like temperature dependent variation in H2wt% and alloying effect on H2wt% and ΔH in different families of alloys. Importantly certain elements like Al, Si, Sc, Cr, and Mn when mixed in small fractions with hydriding elements, systematically reduce ΔH without compromising the storage capacity. Further upon increasing the number of elements in the alloy i.e from binary to ternary

Email address: k.joshi@ncl.res.in (Kavita Joshi*)

to quaternary, the number of compositions with lower enthalpies also increases. From the 6.4 million compositions, we have reported new alloy families having potential for hydrogen storage at room temperature. Finally, we demonstrate that HEART has the potential to scan vast chemical spaces by narrowing down potential materials for hydrogen storage.

Keywords:
Solid-State Hydrogen Storage; Metal Hydrides; Predictive Machine Learning Models; Hydrogen Storage Capacity; Enthalpy of Hydride Formation

1. Introduction

The globe has reached a point where switching to renewable or green energy sources is one of the few viable options for a sustainable environment. Even today, 80% of the world's energy requirements are met by depleting fossil fuels. Therefore, exploring new avenues for environment-friendly energy generation is at the forefront of the research focused on renewable fuel sources.[1, 2] In this milieu of sustainability, hydrogen as an energy carrier is the linchpin in achieving energy security due to its high energy density (142 MJ/Kg).[3, 4, 5] One of the major roadblocks to the hydrogen economy is its economic storage.[6, 7] While compressed and liquefied hydrogen is utilized widely in industries, operational conditions, such as elevated pressure and cryogenic temperature, often restrict its wider usage. Storing hydrogen in a metal or alloys via chemical absorption offers higher volumetric energy densities than compressed gas or liquid hydrogen at ambient conditions.[8, 9]

The storage of hydrogen in metal/alloy is a multi-step process that involves the adsorption of molecular hydrogen, followed by dissociation, penetration, and diffusion through metal lattices to form the hydride. Each step of the process possesses a unique energy barrier that influences the hydrogen storage properties.[10] Further, the energy barrier and the hydrogen storage capacity are both dependent on the absorption temperature as well as pressure. A variety of options ranging from metal organic frameworks, metal hydrides, complex

hydrides, to high entropy alloys (HEA) are explored for solid-state hydrogen storage.[11, 12, 13] As far as storage in metal alloys is concerned, ideally it requires high hydrogen storage capacity, fast kinetics, and favorable thermodynamics at ambient conditions to be economically viable.[14] Despite the promising potential of metal hydrides for hydrogen storage, none of the existing alloys have yet met the targets set by the U.S. Department of Energy for their practical applicability, which indeed underlines the complexity of the problem.

The ability of an alloy to store and release hydrogen is influenced by its composition. Numerous studies have demonstrated that these properties can be modified by altering the relative chemical composition, resulting in a wide range of potential candidates.[15, 16, 17, 18, 19, 20] Therefore, a more comprehensive exploration of the chemical domain is necessary to identify suitable alloys for solid-state hydrogen storage. Conventional screening of chemical space typically entails the intuitive selection of a composition based on domain knowledge, followed by the synthesis and testing of its hydrogen holding capacity at various temperatures and pressures via kinetic study. Generally to measure enthalpy of hydride formation, PCT analysis at different temperatures is carried out.[21] However, these experimental methods are time-consuming and resource-intensive, thereby limiting the number of compositions that can be examined for their suitability as solid-state hydrogen storage materials. In light of this, the development of machine learning models for predicting the hydrogen storage properties of alloys before conducting experiments is a highly promising approach for reducing the chemical space for experimental exploration.

Machine learning is a powerful tool that has been extensively used in various scientific fields to solve complex problems.[22, 23] In the field of solid state hydrogen storage, there are several ML models which have reported valuable insights on factors affecting hydrogen storage properties of metal alloys. For instance, Rahnama et al. developed an ML model that leverages experimental parameters such as the enthalpy of hydride formation, pressure, material class, and temperature to predict the hydrogen storage capacities of metal hydrides. They extended this work to perform a detailed study of the correlation

between these parameters. As expected, their results showed a positive correlation between hydrogen storage capacity, enthalpy of hydride formation, and temperature. They also concluded that material class, temperature, and enthalpy of hydride formation are most influential features for the prediction of hydrogen storage capacity.[24, 25] However, such models use experimental parameters as features and thus cannot be deployed for future predictions. On the other hand, Witman et al. trained gradient boosting regression (GBR) to predict the equilibrium plateau pressure, enthalpy, and entropy of hydride formation using 145 features generated by the Magpie code. Their results reveal that metal hydride equilibrium plateau pressure significantly relies on a volume-based descriptor. Further the model was updated by adding more data and relevant volume and enthalpy-based features to improve its performance for high-throughput screening of high-entropy alloys (HEAs). The updated model was used to predict the equilibrium plateau pressure and enthalpy of hydride formation for 674 equimolar HEAs of refractory elements.[26, 27]. Similarly, Hattrick-Simpers et. al. developed an ML model to estimate the enthalpy of hydrogenation for metal hydrides. They have also used the magpie generated 145 features to train RepTree, Random Forest Regression, and Neural Network models and identified 6110 potential alloys as hydrogen compressors.[28] In summary, these studies demonstrated the use of ML-based models to gain insights and predict thermodynamic properties of metal alloys using simple elementary features. It is pertinent to note that the addition of more relevant features and data set improves model's accuracy. Succeeding this, Suwarno et. al. trained a model to investigate the effect of elements used for alloying on the heat of formation, phase abundance, and H2wt% of the AB2 alloys. ML models like Multivariate Regression, Decision Tree, and Random Forest are trained and tested on 314 data points curated from the literature. Analysis of model has shown that Ni controls the enthalpy of hydride formation, Cr is the significant element determining the phase fraction of the Laves phase C14 and Mn influences the H2wt%. This work demonstrates that how ML-based models bring out the trends depending upon the features used to represent the data.[29] On

similar lines Lu et al. built composition specific ensemble learning method to predict the H2wt% of V-Ti-Cr-Fe alloys. The dataset consist of 81 compositions of V-Ti-Cr-Fe, V-Ti-Fe, V-Ti-Cr, and V-Fe alloys. Model is trained on 19 features consisting of weighted averages of elemental properties along with absorption temperature. Ensemble learning model was able to predict H2wt% with a MAE of 0.187 wt%.[30] Such ML models with high accuracy of prediction highlights the importance of asking appropriate questions and designing suitable features. Needless to note that all models have limitations and there is always a scope for improvement. One of the major limitations of a composition specific model is its transferability to other material classes and compositions. We have compared all the models discussed so far in Table 1 along with the model that we have developed.

ML Model	Feature Set Size	Target	MAE
GBR	145	$\ln(P_{eq})$	1.52[26]
GBR	146	$\ln(P_{eq})$	1.4 [27]
GBR	145	ΔH	6.1 kJ/molH2[26]
GBR	146	ΔH	5.5 kJ/molH2[27]
RF	145	ΔH	8.56 kJ/molH2[28]
RF	8	ΔH	4.36 kJ/molH2[29]
ETR	15	ΔH	5.76 kJ/molH2
NN	5	H2wt%	0.0030 wt%[24]
RF	8	H2wt%	0.101 wt%[29]
Ensemble Method	19	H2wt%	0.187 wt%[30]
ETR	16	H2wt%	0.31 wt%

Table 1: A list of reported ML models for various hydrogen storage properties of metal hydrides. The results from this work are highlighted in red color.

Form Table 1 it is clear that some models have large number of features.[26, 27, 28] Models with smaller feature set are trained on database of specific compositions to understand the variation of hydrogen storage properties as function of composition.[29, 30] Although, these models have better accuracy, since they

are trained on a subset of the data, their transferability is compromised. And hence, could not be effectively used to scan the chemical space. Further H2wt% depends critically on the absorption temperature. None of the models published so far predicted H2wt% as a function of absorption temperature. We attempt to overcome these limitations by designing our feature set by including composition based features which represent key alloy properties, elemental properties that influence the chemical nature of the alloy, DFT based features to account for metal-metal and metal-hydrogen interaction and finally absorption temperature which is the most crucial factor in determining hydrogen storage capacity of any alloy. Based on these newly designed features we have built machine learning models for prediction of hydrogen storage capacity (H2wt%) at different temperatures and enthalpy of hydride formation (ΔH) for multi-component metal alloys.

2. Computational Details

The training dataset is derived from the hydrogen storage material database (HydPARK).[31] The database includes composition, hydrogen storage capacity, enthalpy, and entropy of hydride formation of 2722 alloys. For HYST, all compositions with experimentally measured H2wt% at a given absorption temperature (T) are selected from HydPARK. After preprocessing, the dataset is narrowed to 857 data points across five classes of compositions, viz. AB, A2B, AB2, AB5, SS, and MIC. We have appended this dataset with 105 new points from the literature published after 2005. Thus our dataset contains 962 points in all. To train a model for ΔH, we appended the ML-ready-HydPARK dataset preprocessed by Witman and group. The ML-ready-HydPARK[26] dataset consists of 386 unique compositions of alloys and their enthalpy of hydride formation which is appended with 28 new entries from the literature.

To build a predictive ML model, it is vital to choose/design features which are readily available or easy to calculate. We have computed component-weighted elemental properties as features to describe each composition in the

training set and the search space. The component-weighted elemental properties for a given composition are calculated as: $P = \sum_i c_i p_i$ where c_i is the weight fraction and p_i represents the elemental property of the i^{th} element in a given composition. The designed features can be broadly classified into three classes and are mentioned below:

(1) Fundamental properties of elements: First Ionization Energy (FIE), Electron Affinity (EA), Atomic Density (AD), Atomic Mass (AM), Boiling Point(BP), Heat of Fusion (HF), Specific Heat (SH), Bulk Modulus (BM), Molar Volume (MV), and Thermal Conductivity (TC).

(2) Interactions-based features: The interactions between metal-metal and metal-hydrogen are used as features. These interactions are quantified in terms of bond-energy and bond-length between various metals and hydrogen by employing DFT to compute M-M dimer bond-energy (MM_Eng), M-M dimer bond-length (MM_BL), M-H dimer bond-energy (MH_Eng), and M-H dimer bond-length (MH_BL).

(3) Composition-dependent properties: This class includes features like lattice distortion (atm_sz_diff), the entropy of mixing (dSmix), valance electron concentration (VEC), and electronegativity difference (EN_diff). These features are derived from the Hume-Rothery rules. For a given composition, the resultant structure of the alloy would depend upon magnitude of these parameters. Hence it is expected that in case of a multi-component alloy, the crystal structure and the stability of the alloys will be reflected in these properties. These parameters are used in various machine learning models to predict phases of multi-component alloys successfully.[32, 33], We have incorporated these parameters as features to add more structure-relevant information to our model's learning. The mathematical formulas used for the calculation of these parameters are listed in SI.

(4) Temperature (K): The hydrogen storage capacity varies substantially with absorption temperature and hence absorption temperature is one of the features of HYST, the ML model predicting H2wt% for a given composition. However, the enthalpy of hydride formation is temperature independent, so we

exclude temperature as a feature for THOR.

The Pearson correlation coefficient is computed to identify correlated features and is shown in SI-Fig. 1. The multicollinearity between features may affect the model's performance and makes it difficult to identify the impact of the individual feature on the target property. Therefore, we have examined the correlation matrix for each model to select the right set of features that would enhance learning and uplift the model's predictive performance. Performance of these models as function of cut-off values of correlation coefficients for selecting feature sets is tabulated in SI- Tab. I and II. Based on this analysis we have selected 0.8 as cutoff value of the correlation coefficient for selecting features.

Eight supervised machine learning algorithms from three different categories of linear, kernel, and tree based are evaluated. Since these algorithms are employed on small datasets, they are selected for estimating their performance in predicting hydrogen storage capacity and enthalpy of hydride formation of a given alloy. The three linear models trained to analyze the data are Linear Regression (LR), Ridge Regression (RR), and LASSO, which are the most basic ML models, mapping the linear relationship between an existing input variable and the target property. Following that, the Kernel Ridge Regression (KRR) and Gaussian Process Regression (GPR) algorithms are trained to estimate their performance. These algorithms use a kernel trick to bring out non-linearity in the dataset, reducing calculation tasks and can perform better than linear models for nonlinear data. We also tested three tree-based algorithms, Random Forest Regression (RFR), Extra Tree Regression (ETR), and Gradient Boosting Regression (GBR). These algorithms are chosen for their high predictive ability for nonlinear data paired with ease of interpretation, making complex predictive models much easier to understand.

The scikit-learn python library is used to implement all models. The dataset is rescaled for both linear and kernel-based algorithms using three scalars, StandardScalar, MinMaxScalar, and MaxAbsScalar. GridSearchCV from scikit-learn is used to analyze all possible combinations of hyper-parameter values in order to find the optimal values of hyper-parameters. The dataset is split

into 80-20 ratio for the train and test set. Monte Carlo cross-validation is performed with 100 random train/test splits, i.e., 100 random leave-n-out trials, to assess the model's performance and ensure that it does not over-fit the data. The learning curve is plotted to appraise the model's performance and to check for over-fitting (see SI-Fig. II). The error evaluation metrics, R2 score and Mean Absolute Error (MAE) are used to evaluate the model's performance. All these algorithms are trained and tested for H2wt% and ΔH. Mean absolute error (MAE) and R2 score for all the models are tabulated in SI-Table III and SI-Table IV for H2wt% and ΔH, respectively. After comparing R2 scores and MAEs averaged over 100 iterations for all models on training, testing, and out-of-bag dataset, we selected Extra Tree Regression (ETR) as the final model.

3. Results and Discussions

3.1. Model evaluation and interpretation

Model	MAE Test set	R2 Score Test set	MAE Validation set	R2 Score Validation set
Temperature Independent (H2wt%)	0.35	0.73	0.53	0.64
HYST (H2wt%)	0.31	0.80	0.45	0.81
THOR (kJ/MolH2)	5.76	0.70	4.53	0.89

Table 2: MAE and R2 score for test and validation set of temperature in/dependent H2wt% and ΔH models. Temperature as feature has significantly improved H2wt% prediction.

For H2wt% and ΔH, the tree-based ETR model outperforms other models with lowest MAE and highest R2 score. For H2wt%, the inclusion of temperature as a feature has significantly improved model's performance compared to the temperature-independent model, as tabulated in Table 2. A considerable rise in R2 score for the validation set (unseen data) is observed when temperature is included as one of the features. The average MAE and R2 score for the model predicting enthalpy of the hydride formation turned out to be 5.76 kJ/molH2 and 0.70, respectively. With 15 features we have achieved accuracy

comparable with the published work listed in Table 1. Even though we have trained our models over diverse data of metal alloys, the MAE turned out to be within acceptable limits, indicating better learning, as shown in Figure 1.

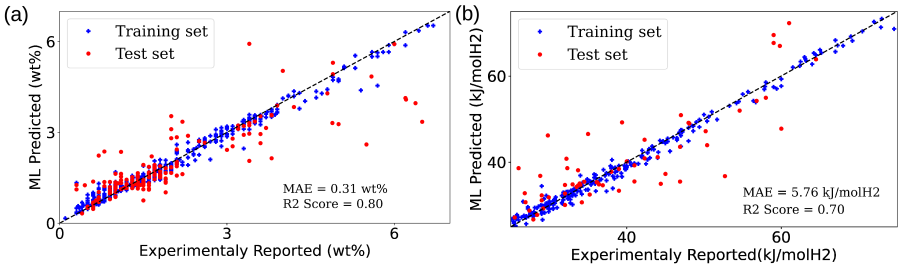

Figure 1: ML predicted versus Experimentally reported (a) H2wt% and (b) ΔH. MAE for the final ETR models cross validated over 100 trials are 0.31 wt% and 5.76 kJ/molH2 respectively.

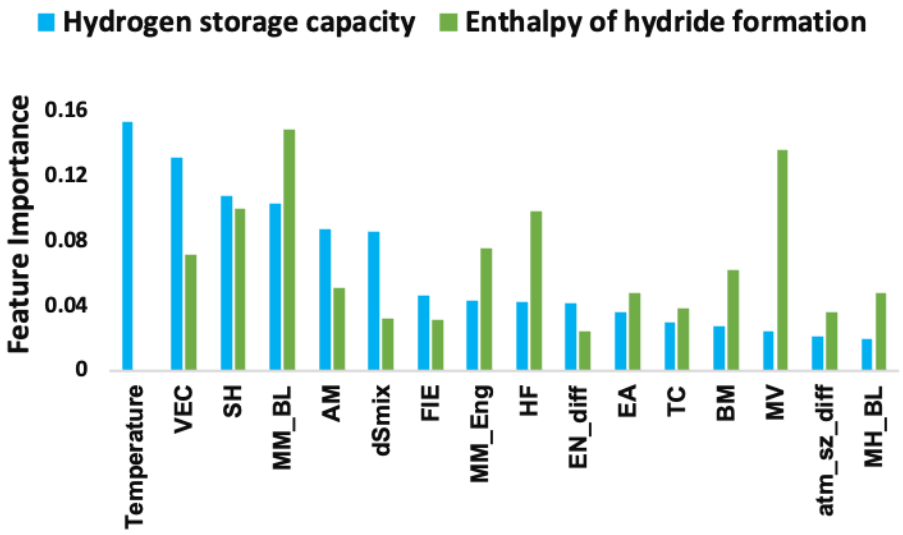

Figure 2: Feature ranking plot by the ETR model for H2wt% and ΔH. The essential features for predicting both properties indicate that the model's learning aligns with the fundamental aspect of hydrogen storage.

Next we plot the feature ranking in descending order of importance (for H2wt%) and averaged over 100 trials (shown in Fig. 2). Same plots with error bars are shown in SI (see SI-Fig. 3 and SI-Fig. 4). Since we are comparing

feature importance of two different properties, error bars are not shown here. Temperature, MM_BL, VEC, SH, Mass, and dSmix are ranked high in predicting the H2wt% of metal alloys. Temperature is an external parameter which helps in boosting the rate of absorption as demonstrated by the variation in the experimentally measured hydrogen storage capacity. Therefore it is an important factor to be considered for more reliable predictions which also reflects in model's feature importance. Apart from temperature, structure of the alloy is also crucial in determining its hydrogen holding capacity. However, structural phases are not known for all the compositions. The features like MM_BL, VEC, Mass, and dSmix are closely associated with the structural phase of the composition and indeed these features have ranked higher. For enthalpy of hydride formation (ΔH), THOR has identified properties like MM_BL, molar volume, bulk modules, specific heat, and the heat of fusion as the most important features. Witman et. al. have also reported volume based descriptor and elastic properties as important features for ΔH which is the take-home message of our model as well. Interestingly the new features derived from DFT to quantify metal-metal and metal-hydrogen interactions are significantly important for predicting both H2wt% and ΔH. Finally, to validate the model's accuracy and

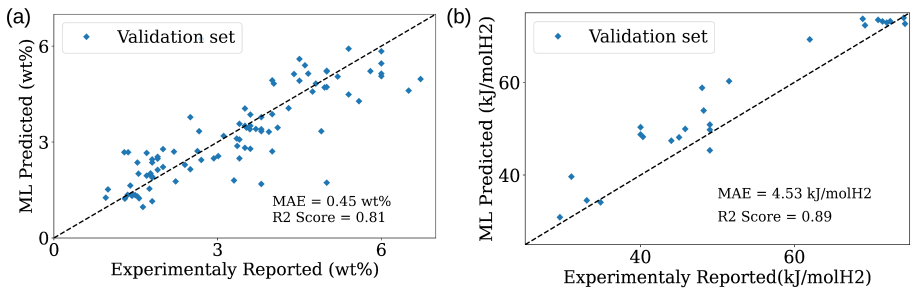

Figure 3: Validation of model's prediction via predicting (a) H2wt% and (b) ΔH for out-of-the-bag compositions

transferability, H2wt% and ΔH are predicted for unseen data. These data sets of H2wt% (105 compositions) and ΔH (28 compositions) are curated from papers published after 2005. These compositions are not part of our training set

and the performance of HYST and THOR is shown in Fig. 3.

Composition	Temperature (K)	Experimentally Reported (wt%)	T-independent model (wt%)	HYST (wt%)
Mg-30wt%LaNi5[34]	470	3.8	5.0	3.78
Mg-30wt%LaNi5[34]	623	4.66	5.0	5.14
Mg88Y12[35]	373	2.63	5.08	2.72
Mg88Y12[35]	423	3.94	5.08	3.32
Mg88Y12[35]	653	6	5.08	5.14

Table 3: Composition, Temperature, experimentally reported H2wt% at that temperature, ML (temperature independent model) predicted H2wt%, and HYST predicted H2wt% are shown in the table to bring out the effect of temperature on the model's performance. In the absence of temperature as one of the features, model predicts same value at different temperatures whereas HYST picks up the variation due to temperature quite well.

Next we demonstrate the importance of including temperature as one of the feature. Values predicted using temperature independent model and HYST are noted in Table 3 and are compared with the experimentally measured H2wt% to demonstrate that HYST has picked up the temperature-dependent variation. As expected, the temperature-independent model could not capture the variation observed in H2wt% with temperature. In contrast, HYST has predicted H2wt% as a function of temperature for a given composition which is at par with the experimentally reported results.

We also note some of the limitations of the model. Figure 4 (a) compares experimentally measured H2wt% (shown as green bars) with those of predicted ones (orange bars) for Mg based alloys which are subset of the validation set. The blue dots (connected with red line) represent the temperature at which H2wt% is measured. A clear trend emerges out. The mismatch between the experimentally measured and predicted values is evident at lower temperatures whereas predictions follow closely experimentally measured values at higher temperatures. This trend could be understood if we examine the data on which the model is trained. In Figure 4 (b), all the Mg based compositions which are part of the training set are shown with their respective H2wt% and corresponding temperature. A closer look at the data brings out the fact that *all* data points

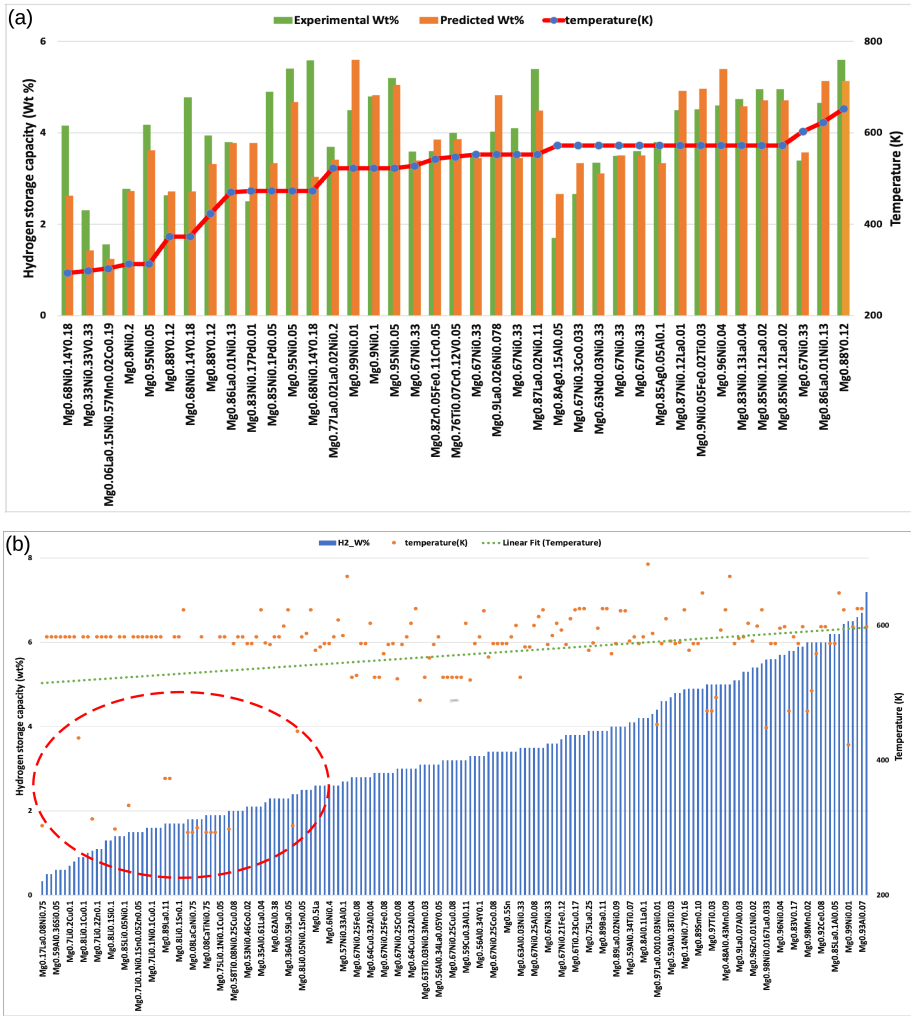

Figure 4: (a) Error bars for predicting a subset of composition for the validation set at different temperatures. Mg-based compositions with lower wt% at high temperatures and higher wt% at low temperatures have higher error bars. (b) The distribution of Mg-based compositions present in our training data, along with their corresponding absorption temperatures. All the data points with lower temperature are marked by circle.

with lower temperature have lower H2wt%. These points are marked by circle to aid an eye. Thus the model gets biased by the input which is reflected in the output by predicting mostly lower H2wt% than the measured ones at lower

temperatures.

We also note that the number of outliers are more in the higher weight percent regions for the testing data of H2wt% model as shown in Figure 1 (a). These outliers can be a result of the insufficient data in the higher weight percent region, and to improve the performance, we added new data points published post HydePARK dataset to the training set which comprised of higher weight percent compositions. On retraining with the appended dataset, we observed that the number of outliers in the test data were reduced as shown in SI-Fig. 5. This again proves that with addition of relevant data we can improve on model's learning. Our second model, THOR, performs well in predicting the enthalpy of hydride formation for the validation set collected from the literature. Comparison between the known and predicted values revealed a lower MAE of 4.53 kJ/molH2. The models are retrained using both archival and hold-out data and used for all subsequent predictions of new compositions.

3.2. Trends in Predicted Hydrogen Storage Properties

To discover new potential hydrogen storage materials, we predicted the hydrogen storage capacity and enthalpy of hydride formation for possible combinations of 38 elements i.e Li, Mg, Ca, Al, Si, Ga, Sn, In, Pb, Sc, Ti, V, Cr, Mn, Fe, Co, Ni, Cu, Zn, Y, Zr, Nb, Mo, Rh, Pd, Ag, Hf, Pt, La, Ce Pr, Nd, Sm, Gd, Tb, Dy, Ho, Er. For these 38 elements, binary, ternary, and quaternary alloy combinations (nC^r) are constructed by varying elemental concentration fraction from 0.05 to 0.95 with a difference of 0.05 for binary alloys and 0.1 to 0.9 with a difference of 0.1 for ternary and quaternary alloys, which accounts to approximately 6.4 million compositions. We employed HYST to predict hydrogen holding capacity at different temperatures and THOR to predict enthalpy of hydride formation for these 6.4 million compositions. What follows next are the trends observed and insights gained from these predictions.

Figure 5 illustrates the relative percentage (noted in red color) and the number of compositions in a specific class (noted in black color) over the range of wt% at different temperatures for scanned compositions. For binary, ternary,

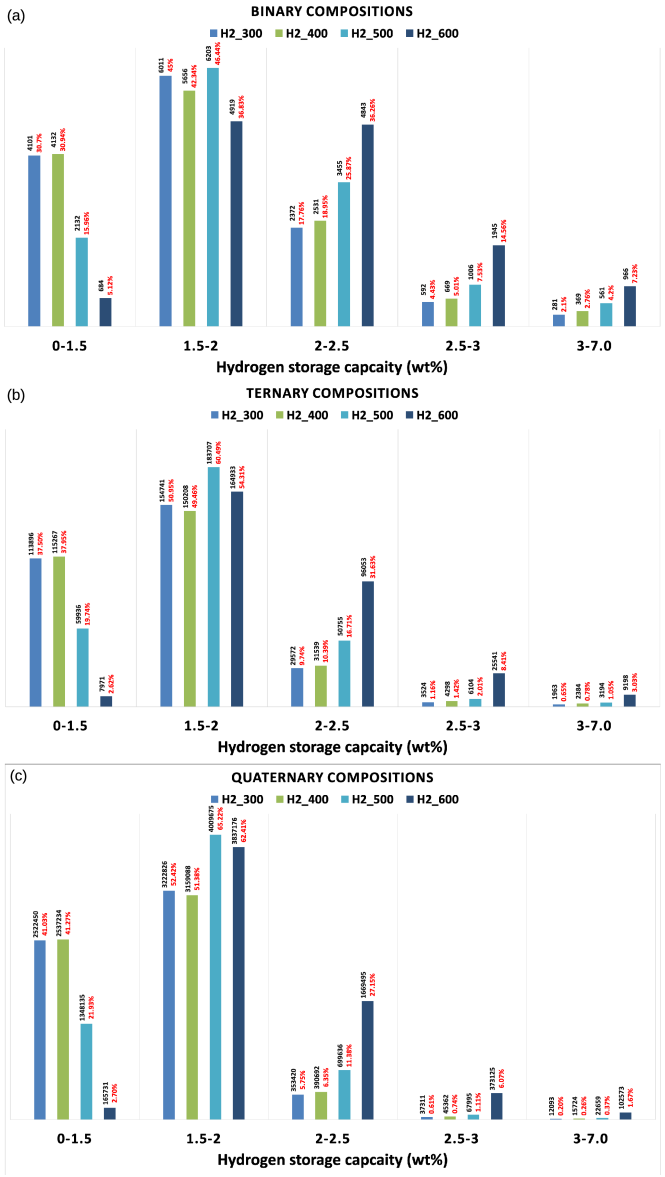

Figure 5: (a), (b), and (c) Plot of the relative percentage of compositions (noted in red color) and number of compositions in a specific class (noted in black color) over the range of wt% at different temperatures for binary, ternary, and quaternary alloys, respectively. A gradual shift towards higher H2wt% is observed with increasing temperature, i.e. from 300K to 600K.

and quaternary alloys, maximum number of compositions are observed with H2wt% between 1.5 to 2 wt% irrespective of the absorption temperature as shown in Figure 5 (a), (b), and (c). Moreover, as temperature increases, the number of compositions with higher H2wt% increases. For instance, while only about 2% of binary compositions have H2wt% between 3-7 wt% at 300K, this rises to above 7% at 600K. Similar trends are observed for H2wt% range 2-2.5 wt% and 2.5-3 wt%. Since total number of compositions is same, the reverse trend is observed for lower wt% ranges i.e. with increasing temperature the number of compositions with lower H2wt% decreases i.e between 0-1.5. Another important point to be noted is that although the relative percentage of ternary and quaternary compositions at higher H2wt% (i.e. > 2.5) is less (compared to that of binary alloys) the actual number of such compositions is substantially more. Total number of ternary alloy compositions scanned are 3,03,714 and the number of compositions with H2wt% more than 2.5 is 5487 at room temperature. The number increases to 34709 at 600K as shown in Figure 5 (b). Interestingly for quaternary alloys, the relative number of compositions with higher wt% have also increased substantially. About 49404 compositions have H2wt% > 2.5 at 300K and the number shoots up to more than 400,000 at 600K as shown in Figure 5 (c). In Fig. 6 enthalpy of hydride formation is plotted for binary, ternary, and quaternary alloys. Compositions having ΔH less than 40 kJ/molH2 or more than 60 kJ/molH2 are less in number, and the maximum number of compositions fall in the range of 40-60 kJ/molH2. Although for all types of alloys (binary, ternary, and quaternary) the peak lies in the range of 40-50 kJ/molH2, a closer look brings out an interesting observation. With increasing number of elements in the alloys, the enthalpy of hydride formation decreases. For example, percentage of alloys with ΔH between 40-50 kJ/molH2 increases as we move from binary to ternary to quaternary. Also, as we move from binary to ternary and then to quaternary, the number of alloy compositions having H2wt% > 2.5 at relatively lower ΔH is increasing as shown in Figure 7, which signify how alloying of different elements results in a material with modified hydrogen storage properties. Overall, out of 6.4 million compositions

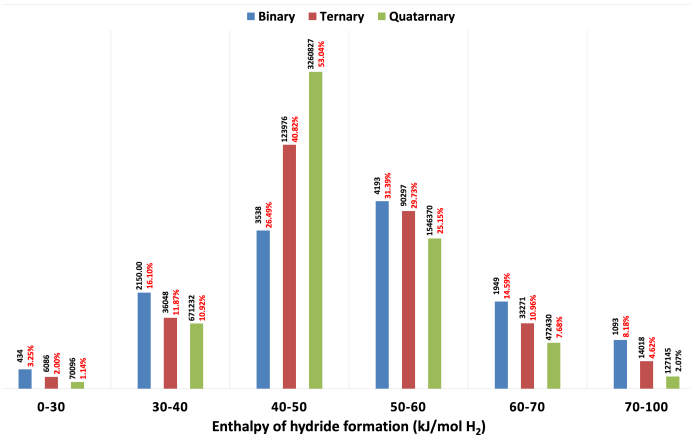

Figure 6: A plot of the relative percentage of binary, ternary, and quaternary compositions in different range of ΔH. A maximum number of compositions are observed in the 40-60 kJ/molH2 of ΔH range.

there are more than 55000 compositions which are having H2wt% > 2.5 at room temperature and more than 786000 compositions which are having enthalpy $<$ 40 kJ/molH2.

We need to understand these numbers with caution. Right now the variation in the composition is carried out with step of 0.1 (or 10% change in the fraction). This is chosen arbitrarily and if it is reduced further to 0.05 or increased to 0.2, the actual number will change accordingly.

3.3. Prediction of New Alloys Families: Insights from Machine Learning

Series	Elements
Metals	Si, Li, Mg, Ca, Ga, Sn, Pb, In, Al
Transition metals	Zn, Hf, V, Mn, Y, Zr, Sc, Rh, Nb, Pd, Cu, Cr, Ni, Ti, Pt, Fe, Co, Mo, Ag
Lanthanides	La, Dy, Tb, Er, Ce, Sm, Ho, Pr, Nd, Gd

Table 4: 38 elements classified into three classes metals, transition metals, and lanthanides. Metals could be further classified as metalloid (Si), alkali metal (Li), alkaline earth metal (Ca), poor metals (Ga, Pb, In, and Al)

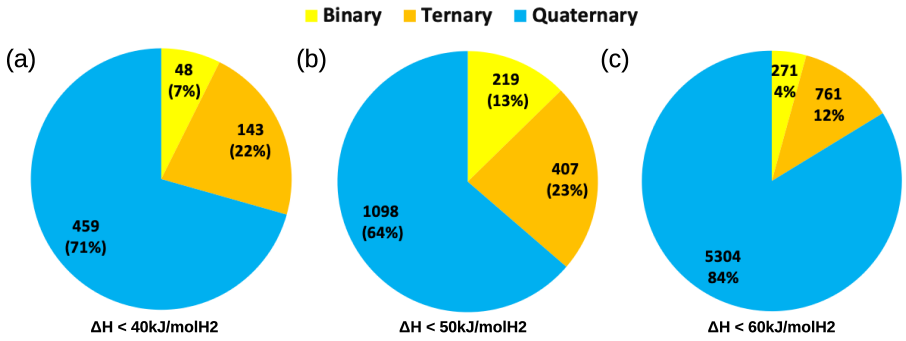

Figure 7: Distribution of number of composition having H2wt% > 2.5wt% with (a) ΔH < 40 kJ/molH2, (b) ΔH < 50 kJ/molH2 and (c) ΔH < 60 kJ/molH2 in three classes of binary, ternary, and quaternary alloys. For a given cutoff of H2wt% and ΔH the number of alloy compositions having relatively lower ΔH are increasing with number of elements in an alloy.

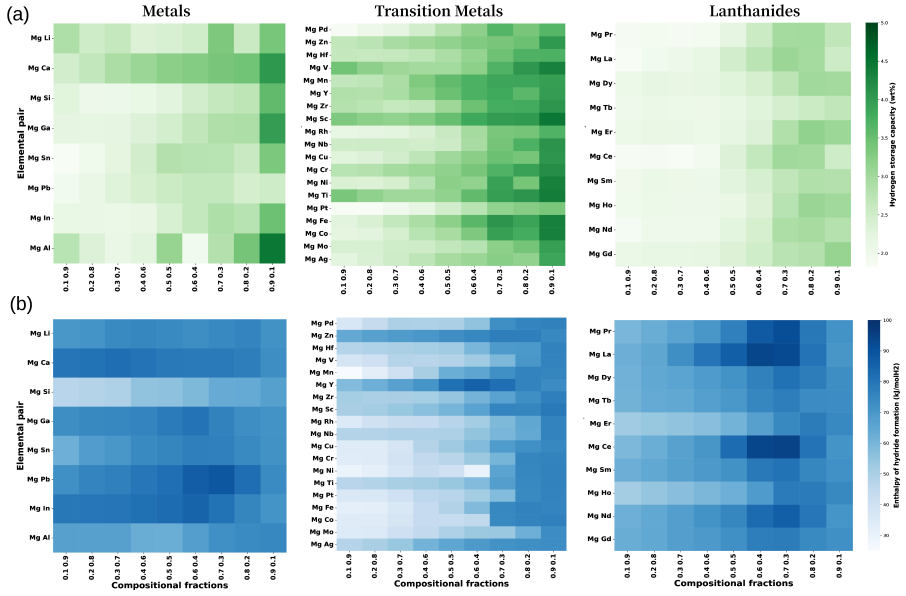

Figure 8: Heat map representing (a) H2wt% at 300(K) and (b) ΔH of Mg-based system when mixed with metals, transition metals and lanthanides.

We analyze the predicted properties to identify systematic chemical trends that are exhibited by various compositions of the prediction set. First, we

classified the 38 selected elements into three distinct classes, as listed in Table 4. Next, we plot the elements from each series against the others to determine the influence of alloying on predicted properties. The Figure 8 (a) shows the systematic change in H2wt% at room temperature due to alloying of Mg with elements from different series. Alloying with poor metals like Ga, Sn, Pb, and In, all lanthanides and late transition metals like Rh, Pt, Ag, and Hf in Mg-based alloy results into poor hydrogen holding capacity. These elements are larger in size and have poor affinity towards hydrogen which makes them poor substituents to enhance hydrogen storage capacity. On the other hand elements like Al, Ca, Sc, V, Ti, Co, Cr, Mn, Fe, Co, Zr, and Y have shown improved hydrogen holding capacity when alloyed with Mg at room temperature. It is also observed in previous studies that when these elements are alloyed with Mg, they alter the crystal structure and composition of the Mg based alloy which leads to an ease of hydrogen ab/desorption even at lower temperatures.[36, 37] For simplicity, here we explained only the trends observed for Mg when alloyed with the other 37 elements. However in supplementary information we have also examined the effect of alloying on other hydriding elements like Li, Ti, and V. Trends in predicted H2wt% and ΔH for Li, Ti, and V when alloyed with the other 37 elements are shown in the SI-Fig. 6, SI-Fig. 7, and SI-Fig. 8 respectively.

The change in enthalpy of hydride formation due to alloying of Mg with elements from different series is shown in the Figure 8 (b). In general, ΔH falls somewhere inbetween enthalpy of hydride formation of the constituent elements. This trend has been observed in predicted ΔH. The plot shows that increasing concentration of non-hydriding elements like Si, Sn, Cu, Cr, Ni, Fe, Co, Mo, Er, and Ho reduces the ΔH of the resulting alloy. On the other hand mixing of two hydriding elements like Mg with Li, Ca, Pb, Y, Zn, Y, La and Ce leads to enhanced stability with higher ΔH. This observation is consistent with experimentally observed values of the enthalpy of hydride formation in many alloys like ZrCr1.8, TiCr1.8, NaAl etc.[38] It is also important to mention that the extent of change in H2wt% and ΔH varies with elements. We have observed

the addition of small fraction of Al, Sc, Cr, Ti, Mn, Fe, Y, Nb, and Pd leads to drastic reduction in enthalpy along with improved hydrogen holding capacity. This shows that the model has picked up the chemical trends existed in training data and interpolate well while predicting.

3.4. New Composition Family

We filtered the 6.4 million compositions based on their predicted hydrogen storage properties to 6480 potential compositions at 300K which satisfied the criteria set by the DOE for stationary applications. The DOE specifies that materials for stationary application should have a H2wt% > 2.5 at room temperature and ΔH < 60 kJ/molH2.[39] These 6480 compositions have met these criteria and show promising potential for hydrogen storage applications. Through the analysis of 6480 binary, ternary, and quaternary alloys, we have identified several promising families of alloys that exhibit potential for further investigation. Among the binary alloys, 276 compositions comprising 53 different elemental pairs were found to satisfy the criteria. Of these pairs, seven V-XX pairs (where XX represents Cr, Ti, Sc, Nb, Ga, Mn, and Fe) exhibited H2wt% > 3, and ΔH < 45 kJ/molH2. The aforementioned predictions align with the trends experimentally reported in the existing literature for V-Ti, V-Cr, and V-Mn binary alloys. However, our model has also predicted some new binary compositions, such as V-Sc, V-Nb, and V-Ga, that exhibit promising hydrogen storage properties and warrant further experimental investigation. In the class of ternary alloys, over 700 compositions were identified that satisfy the criteria of H2wt% > 2.5 and ΔH < 60 kJ/MolH2. Furthermore, more than 50 compositions of V-Ti-X, Mg-Ti-X, and V-Mg-X alloys (where X represents Cr, Ni, Co, Fe, Mn, and Sc) exhibited H2wt% > 3. Our predictions are consistent with previous experimental values of these parameters for V-Ti-Cr, V-Cr-Mn, and Ti-Cr-Mn ternary alloy families.[40, 41, 42] Additionally, Mg-Ti-X and V-Mg-X (where X represents Cr, Ni, Co, Fe, Mn, and Sc) are new families that have not yet been explored but exhibit promising hydrogen storage properties at room temperature.

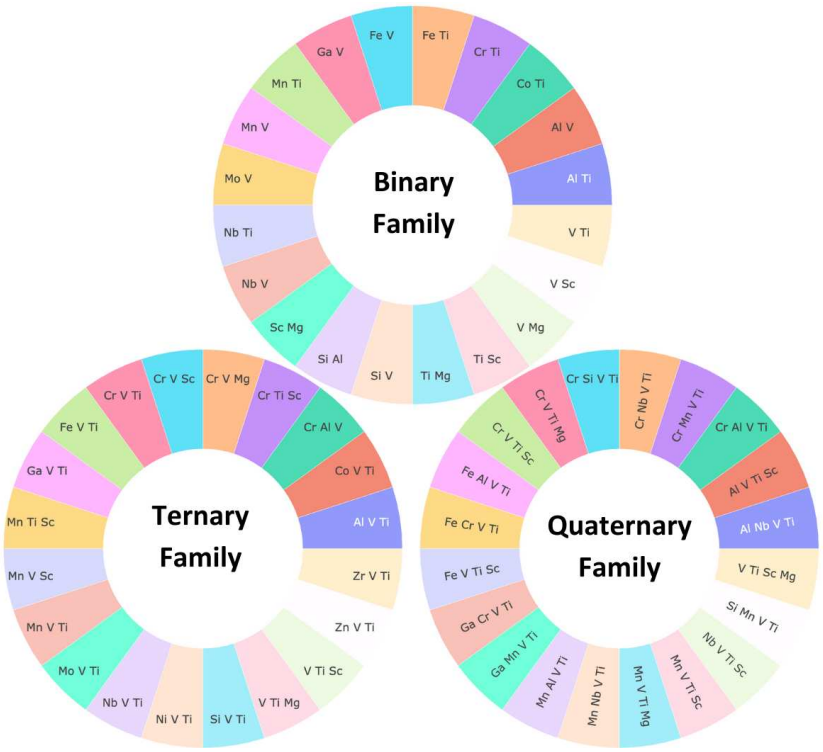

Figure 9: List of promising families of binary, ternary, and quaternary metal alloys compositions for solid state hydrogen storage at room temperature.

In the class of quaternary alloy, more than 5500 compositions are satisfying stationary storage criteria and more than 200 compositions are having H2wt% > 3. Alloy families, V-Ti-YY, Mg-Fe-YY, Mg-Ti-YY, Mg-La-YY, Mg-Ce-YY, and Mg-V-YY, where YY represents Fe-Al, Fe-Cr, Si-Sm, Si-Y, Cr-Mn, Si-Mn, and Al-Cr had a H2wt% > 3 and $\Delta H < 50$ kJ/molH2. We also predict some interesting new families like Mg-V-Ti-YY, V-Ti-Cr-YY, and V-Ti-Al-YY, where YY represents Fe, Sc, Nb, Si, and Mn. Overall, the analysis shows that there are many compositions of binary, ternary, and quaternary alloys that have the potential to be explored further for hydrogen storage. For now, we have represented pictorially 20 families in Figure 9 from each class that show potential for hydrogen storage application at room temperature. These families can be further explored and studied in detail to identify the most promising

compositions for practical use in hydrogen storage applications.

4. Conclusion

In this work, we have designed HEART, a machine learning framework, for prediction of H2wt% at different temperatures (HYST) and ΔH (THOR) of multicomponent metal alloys. Both models demonstrate good predictive accuracy for validations set (HYST: R2 score = 0.81 and MAE = 0.45 wt%; THOR R2 score = 0.89 and MAE = 4.53 kJ/molH2). The study also highlights the significance of incorporating more data as well as relevant features such as temperature, metal-metal, metal-hydrogen interactions and compositional based features along with elemental properties to enhance the models' learning. Addition of temperature as a feature in the HYST model has an added advantage of predicting the H2wt% of an alloy as a function of temperature. We flagged limitation in the model's learning due to inadequate data and subsequent improvement in it with addition of more relevant data in the training set. Therefore, it is necessary to build an updated dataset specifically for solid-state hydrogen storage. Furthermore, addition of alloy's structural information as feature can enhance the model's predictability. We constructed 6.4 million multi-component (binary, ternary, and quaternary) compositions and used the trained ML models to predict H2wt% at 300K, 400K, 500K, and 600K along with ΔH. Significant and systematic changes have been observed in alloys' predicted H2wt% and ΔH as a function of temperature, compositional fraction, and constituent elements. Following are the trends observed:

- H2wt% of an alloy increases with the absorption temperature across all the predicted alloy classes. The number of compositions in the higher H2wt% region increases with temperature from 300-600K.

- For ΔH, with an increase in the number of constituents elements in the alloy, i.e. as we move from binary to ternary to quaternary, the ΔH decreases.

- Predicted hydrogen storage capacity and enthalpy of hydrogenation are significantly affected by the addition of non-hydriding or hydriding elements in a different manner.

- These distinct variations of predicted hydrogen storage properties are attributed to the elemental and compositional features incorporated during the models' training.

- Compositions comprising light elements like Li, Mg, Al, etc., have high H2wt% and ΔH which is an inherent property of light metal hydrides. The H2wt% of these compositions increases significantly with temperature.

- Compositions with constituent heavier elements like Mo, Rh, Pd, Ag, Hf, and Pt fall in the lower H2wt% range, i.e., less than 1.5 wt%, even at an elevated temperature of 600K. This shows that temperature has a negligent effect on the H2wt% of these compositions.

- Temperature-dependent variation of H2wt% of compositions also gives us insights about the combination of elements to look for with enhanced H2wt% in different temperature regions.

- The models' predictions are in line with the experimental trends of destabilization using non-hydriding elements. Specifically, when small amounts of a subset of non-hydriding elements, such as Cr, Fe, Cu, Ni, Co, Si, and Sn, are alloyed with hydriding elements like Mg, Al, V, and Ti, ΔH is decreased without significantly impacting H2wt%.

Finally, our predictions pin pointed 6480 compositions which satisfies the stationary storage target properties set by DOE (H2wt% $>$ 2.5 at 300 K and ΔH $<$ 60 kJ/molH2). From the analysis of 6480 compositions (binary, ternary, and quaternary alloys), we have reported promising families of alloys that can be selected for further experimental investigation. This study demonstrates how ML models can expedite the process of materials discovery, even for alloys.

Conflicts of interest

"There are no conflicts to declare".

Acknowledgements

Authors thank Professor Sushant Kumar (IIT-Patna) for many fruitful discussions. CSIR is acknowledged for financial support through grant HCP-44-05 (HEART). CSIR-4PI is acknowledged for the computational facility. AV thanks DST for INSPIRE fellowship.

References

[1] D. Gielen, F. Boshell, D. Saygin, M. D. Bazilian, N. Wagner, R. Gorini, The role of renewable energy in the global energy transformation, Energy Strategy Reviews 24 (2019) 38–50.

[2] P. A. Owusu, S. Asumadu-Sarkodie, A review of renewable energy sources, sustainability issues and climate change mitigation, Cogent Engineering 3 (2016) 1167990.

[3] S. van Renssen, The hydrogen solution?, Nature Climate Change 10 (2020) 799–801.

[4] K. Espegren, S. Damman, P. Pisciella, I. Graabak, A. Tomasgard, The role of hydrogen in the transition from a petroleum economy to a low-carbon society, international journal of hydrogen energy 46 (2021) 23125–23138.

[5] D. Parra, L. Valverde, F. J. Pino, M. K. Patel, A review on the role, cost and value of hydrogen energy systems for deep decarbonisation, Renewable and Sustainable Energy Reviews 101 (2019) 279–294.

[6] A. M. Abdalla, S. Hossain, O. B. Nisfindy, A. T. Azad, M. Dawood, A. K. Azad, Hydrogen production, storage, transportation and key challenges with applications: A review, Energy conversion and management 165 (2018) 602–627.

[7] A. Züttel, Materials for hydrogen storage, Materials today 6 (2003) 24–33.

[8] J. B. Von Colbe, J.-R. Ares, J. Barale, M. Baricco, C. Buckley, G. Capurso, N. Gallandat, D. M. Grant, M. N. Guzik, I. Jacob, et al., Application of hydrides in hydrogen storage and compression: Achievements, outlook and perspectives, international journal of hydrogen energy 44 (2019) 7780–7808.

[9] A. Kumar, P. Muthukumar, P. Sharma, E. A. Kumar, Absorption based solid state hydrogen storage system: A review, Sustainable Energy Technologies and Assessments 52 (2022) 102204.

[10] Q. Lai, Y. Sun, T. Wang, P. Modi, C. Cazorla, U. B. Demirci, J. R. Ares Fernandez, F. Leardini, K.-F. Aguey-Zinsou, How to design hydrogen storage materials? fundamentals, synthesis, and storage tanks, Advanced Sustainable Systems 3 (2019) 1900043.

[11] J. Yang, A. Sudik, C. Wolverton, D. J. Siegel, High capacity hydrogen storage materials: attributes for automotive applications and techniques for materials discovery, Chemical Society Reviews 39 (2010) 656–675.

[12] M. Sahlberg, D. Karlsson, C. Zlotea, U. Jansson, Superior hydrogen storage in high entropy alloys, Scientific Reports 6 (2016) 1–6.

[13] H. Reardon, J. M. Hanlon, R. W. Hughes, A. Godula-Jopek, T. K. Mandal, D. H. Gregory, Emerging concepts in solid-state hydrogen storage: the role of nanomaterials design, Energy & Environmental Science 5 (2012) 5951–5979.

[14] B. P. Tarasov, P. V. Fursikov, A. A. Volodin, M. S. Bocharnikov, Y. Y. Shimkus, A. M. Kashin, V. A. Yartys, S. Chidziva, S. Pasupathi, M. V. Lototskyy, Metal hydride hydrogen storage and compression systems for energy storage technologies, International Journal of Hydrogen Energy 46 (2021) 13647–13657.

[15] N. Hanada, T. Ichikawa, H. Fujii, Catalytic effect of nanoparticle 3d-transition metals on hydrogen storage properties in magnesium hydride

mgh2 prepared by mechanical milling, The Journal of Physical Chemistry B 109 (2005) 7188–7194.

[16] A. Kumar, S. Banerjee, C. Pillai, S. Bharadwaj, Hydrogen storage properties of Ti2- xCrVMx (M= Fe, Co, Ni) alloys, International journal of hydrogen energy 38 (2013) 13335–13342.

[17] R. C. Muduli, P. Kale, Silicon nanostructures for solid-state hydrogen storage: A review, International Journal of Hydrogen Energy 48 (2023) 1401–1439.

[18] Y. Zhao, R. Li, R. Tang, B. Li, R. Yu, W. Liu, H. Kou, J. Meng, Effect of Ti substitution on hydrogen storage properties of Zr1-xTixCo (x= 0, 0.1, 0.2, 0.3) alloys, Journal of energy chemistry 23 (2014) 9–14.

[19] V. Kumar, P. Kumar, S. Pati, P. Sharma, K. Takahashi, Tuning the hydrogen storage properties of TiFe clusters via Zr substitution, Energy Storage 2 (2020) e157.

[20] P. Meena, R. Singh, V. Sharma, I. Jain, Role of NiMn9. 3Al4. 0Co14. 1Fe3. 6 alloy on dehydrogenation kinetics of MgH2, Journal of Magnesium and Alloys 6 (2018) 318–325.

[21] K. J. Gross, K. R. Carrington, S. Barcelo, A. Karkamkar, J. Purewal, S. Ma, H.-C. Zhou, P. Dantzer, K. Ott, Y. Pivak, et al., Recommended best practices for the characterization of storage properties of hydrogen storage materials, Tech. rep., EMN-HYMARC (EMN-HyMARC); National Renewable Energy Lab.(NREL), Golden, CO(United States) (2016).

[22] D. Rangel-Martinez, K. Nigam, L. A. Ricardez-Sandoval, Machine learning on sustainable energy: A review and outlook on renewable energy systems, catalysis, smart grid and energy storage, Chemical Engineering Research and Design 174 (2021) 414–441.

[23] S. M. Moosavi, K. M. Jablonka, B. Smit, The role of machine learning in the understanding and design of materials, Journal of the American Chemical Society 142 (2020) 20273–20287.

[24] A. Rahnama, G. Zepon, S. Sridhar, Machine learning based prediction of metal hydrides for hydrogen storage, part I: Prediction of hydrogen weight percent, International Journal of Hydrogen Energy 44 (2019) 7337–7344.

[25] A. Rahnama, G. Zepon, S. Sridhar, Machine learning based prediction of metal hydrides for hydrogen storage, part II: Prediction of material class, International Journal of Hydrogen Energy 44 (2019) 7345–7353.

[26] M. Witman, S. Ling, D. M. Grant, G. S. Walker, S. Agarwal, V. Stavila, M. D. Allendorf, Extracting an empirical intermetallic hydride design principle from limited data via interpretable machine learning, The Journal of Physical Chemistry Letters 11 (2019) 40–47.

[27] M. Witman, G. Ek, S. Ling, J. Chames, S. Agarwal, J. Wong, M. D. Allendorf, M. Sahlberg, V. Stavila, Data-driven discovery and synthesis of high entropy alloy hydrides with targeted thermodynamic stability, Chemistry of Materials 33 (2021) 4067–4076.

[28] J. R. Hattrick-Simpers, K. Choudhary, C. Corgnale, A simple constrained machine learning model for predicting high-pressure-hydrogen-compressor materials, Molecular Systems Design & Engineering 3 (2018) 509–517.

[29] S. Suwarno, G. Dicky, A. Suyuthi, M. Effendi, W. Witantyo, L. Noerochim, M. Ismail, Machine learning analysis of alloying element effects on hydrogen storage properties of ab2 metal hydrides, International Journal of Hydrogen Energy 47 (2022) 11938–11947.

[30] Z. Lu, J. Wang, Y. Wu, X. Guo, W. Xiao, Predicting hydrogen storage capacity of V–Ti–Cr–Fe alloy via ensemble machine learning, International Journal of Hydrogen Energy 47 (2022) 34583–34593.

[31] US DOE hydrogen storage database, http://hydrogenmaterialssearch.govtools.us/, accessed: 2023-04-07.

[32] Z. Zhou, Y. Zhou, Q. He, Z. Ding, F. Li, Y. Yang, Machine learning guided appraisal and exploration of phase design for high entropy alloys, npj Computational Materials 5 (2019) 128.

[33] Y. Zhang, C. Wen, C. Wang, S. Antonov, D. Xue, Y. Bai, Y. Su, Phase prediction in high entropy alloys with a rational selection of materials descriptors and machine learning models, Acta Materialia 185 (2020) 528–539.

[34] B. Sakintuna, F. Lamari-Darkrim, M. Hirscher, Metal hydride materials for solid hydrogen storage: a review, International journal of hydrogen energy 32 (2007) 1121–1140.

[35] T. Yang, Z. Yuan, W. Bu, Z. Jia, Y. Qi, Y. Zhang, Evolution of the phase structure and hydrogen storage thermodynamics and kinetics of mg88y12 binary alloy, International Journal of Hydrogen Energy 41 (2016) 2689–2699.

[36] J. Lu, Y. J. Choi, Z. Z. Fang, H. Y. Sohn, E. Ronnebro, Hydrogen storage properties of nanosized MgH2- 0.1 tih2 prepared by ultrahigh-energy- high-pressure milling, Journal of the American Chemical Society 131 (2009) 15843–15852.

[37] D. Vyas, P. Jain, G. Agarwal, A. Jain, I. Jain, Hydrogen storage properties of Mg2Ni affected by Cr catalyst, International journal of hydrogen energy 37 (2012) 16013–16017.

[38] A. Andreasen, Predicting formation enthalpies of metal hydrides (2004). URL https://www.osti.gov/etdeweb/servlets/purl/20553542

[39] P. Modi, K.-F. Aguey-Zinsou, Room temperature metal hydrides for stationary and heat storage applications: A review, Frontiers in Energy Research 9 (2021) 616115.

[40] R. B. Strozi, D. R. Leiva, G. Zepon, W. J. Botta, J. Huot, Effects of the chromium content in (TiVNb)100-xCrx body-centered cubic high entropy alloys designed for hydrogen storage applications, Energies 14 (2021) 3068.

[41] X. Chen, R. Chen, X. Ding, H. Fang, J. Guo, H. Ding, Y. Su, H. Fu, Crystal structure and hydrogen storage properties of Ti-V-Mn alloys, International Journal of Hydrogen Energy 43 (2018) 6210–6218.

[42] W. Li, E. Wu, P. Ma, K. Sun, D. Chen, Hydrogen storage properties of Ti1- xScxMnCr laves phase alloys, International journal of energy research 37 (2013) 686–697.

Supporting Information

Solid state hydrogen storage: Decoding the path through machine learning

(Dated: April 22, 2023)

I. FEATURE SELECTION

The performance of machine learning models are evaluated with regards to various sets of collinear features as shown in Figure 1. Collinear features refer to the variables that share a high degree of correlation among each other. The presence of such features in a model can lead to redundancy and over-fitting, thereby deteriorating the model's performance.

To assess the impact of collinearity on the performance of both the models, the results

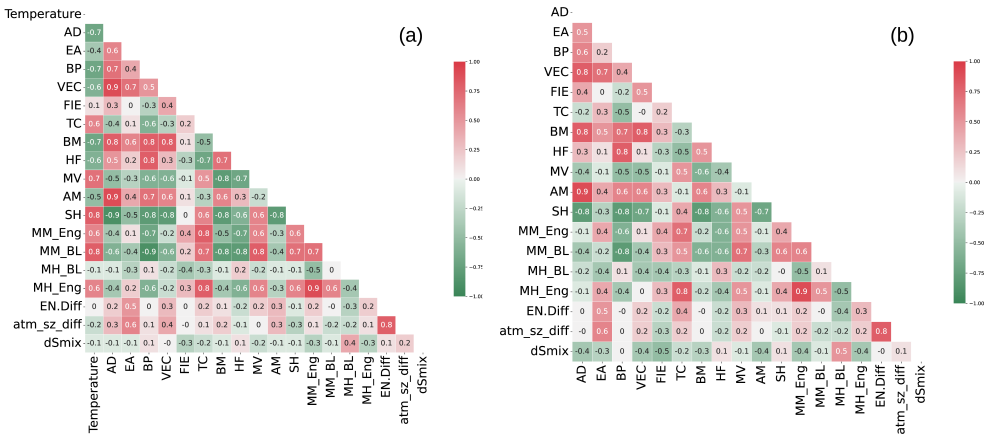

FIG. 1. Pearson's correlation matrix of feature vector set for (a) HYST (b) THOR. The matrix shows the pair correlation between the properties.

are analyzed and presented in Table I and Table II. The results revealed that features with high collinearity (0.9) such as Atomic Density, Boiling Point, and MH_Eng, had minimal effect on the model's performance when excluded from the model. However, the removal of additional features beyond this point resulted in a decline in the model's performance. Hence, it is crucial to carefully select the relevant features by removing as many collinear features as feasible in order to achieve a trade-off between accuracy and interpretability.

Composition dependent properties are calculated using the following formulas.

$$VEC = \sum_{i=1}^{n} c_i VEC_i$$

$$EN\_diff = \sqrt{\sum_{i=1}^{n} c_i(\chi_i - \bar{\chi})^2}$$

$$atm\_sz\_diff = 100 \times \sqrt{\sum_{i=1}^{n} c_i(1 - \frac{r_i}{\bar{r}})^2}$$

$$dSmix = -R \sum_{i=1}^{n} c_i \ln c_i$$

TABLE I. Feature selection for H2wt% model. Maximum collinearity represents the cut-off used to limit the number of features. Number in () represent number of features in a set.

Maximum collinearity	Features	MAE Test set	R2 Score Test set	MAE Validation set	R2 Score Validation set
0.9 (19)	Temperature, AD, EA, BP, VEC, FIE, TC, BM, HF, MV, AM, SH, MM_Eng, MM_BL, MH_BL, MH_Eng, EN.Diff, atm_sz_diff, dSmix	0.31	0.80	0.43	0.81
0.8 (16)	Temperature, EA, VEC, FIE, TC, BM, HF, MV, AM, SH, MM_Eng, MM_BL, MH_BL, EN.Diff, atm_sz_diff, dSmix	0.31	0.80	0.44	0.81
0.7 (8)	Temperature, EA, VEC, FIE, AM, MH_Eng, EN.Diff, dSmix	0.31	0.80	0.49	0.75
0.6 (7)	Temperature, VEC, FIE, AM, MH_Eng, EN.Diff, dSmix	0.33	0.78	0.49	0.75

TABLE II. Feature selection for ΔH model. Maximum collinearity represents the cut-off used to limit the number of features. Number in () represent number of features in a set.

Maximum collinearity	Features	MAE Test set	R2 Score Test set	MAE Validation set	R2 Score Validation set
0.9 (18)	AD,EA, BP,VEC, FIE,TC, BM, HF, MV, AM, SH, MM_Eng, MM_BL, MH_BL, MH_Eng, EN.Diff, atm_sz_diff, dSmix	5.80	0.70	4.55	0.88
0.8 (15)	EA, VEC, FIE, TC, BM, HF, MV, AM, SH, MM_Eng, MM_BL, MH_BL, EN.Diff, atm_sz_diff, dSmix	5.76	0.70	4.53	0.89
0.7 (12)	EA, VEC, FIE, HF, MV AM, SH, MM_Eng, MM_BL, MH_BL, EN.Diff, dSmix	5.91	0.68	4.57	0.86
0.6 (9)	VEC, FIE, HF, SH, MM_Eng, MM_BL, MH_BL, EN.Diff, dSmix	6.11	0.68	4.98	0.84

where c_i represents the fraction of the constituent i^{th} element, VEC_i represents the valence electron concentration of the i^{th} element, χ_i represents the electronegativity of the i^{th} element, $\bar{\chi}$ represents the average electronegativity of all the constituent elements, r_i represents

the radius of the i^{th} element, $\bar{r}$ represents the average radius of the constituent elements and R represents the gas constant.

II. MODEL SELECTION

The process of developing a model for obtaining the desired properties involves extensive testing and evaluation of multiple models. In this context, eight different algorithms were subjected to rigorous testing to identify the most suitable one for the desired properties. To evaluate the performance of each model, the average Mean Absolute Error (MAE) and R2 score were computed for the train, test, and validation sets over 100 trials, and the results were recorded in Table III and Table IV.

TABLE III. Evaluation of machine learning models for H2wt%. ETR is selected as the final model.

Class	Algorithm	MAE Test set	R2 Score Test set	MAE Validation set	R2 Score Validation set
Linear	LR	0.49	0.46	1.36	-0.45
	RR	0.48	0.61	1.32	-0.38
	LASSO	0.48	0.49	1.33	-0.39
Kernel	KRR	0.31	0.76	1.24	0.044
	GPR	0.36	0.71	2.86	-2.3
Tree	GBR	0.32	0.74	0.50	0.70
	RF	0.33	0.75	0.48	0.75
	ETR	0.31	0.80	0.43	0.81

Analysis of the results revealed that linear models performed poorly in predicting both H2wt% and enthalpy of hydride formation. The complexity of these properties could be a reason for this poor performance since linear models are not well-suited to capture complex relationships between variables. On the other hand, kernel models performed better during training and testing, however they performed with low accuracy for the validation set. Tree-based models demonstrated relatively better performance than linear and kernel models during training, testing, and validation. Upon closer inspection of the performance metrics, it was found that RF and ETR models had similar performance. However, ETR was selected as the final algorithm because it demonstrated the lowest MAE and highest R2 score during training and testing for both properties, i.e., H2wt% and ΔH.

TABLE IV. Evaluation of machine learning models for enthalpy of hydride formation (ΔH). ETR is selected as the final model.

Class	Algorithm	MAE Test set	R2 Score Test set	MAE Validation set	R2 Score Validation set
Linear	LR	7.36	0.40	12.81	0.05
	RR	7.96	0.47	12.52	0.23
	LASSO	7.84	0.5	8.43	0.68
Kernel	KRR	7.02	0.46	13.14	0.044
	GPR	7.0	0.61	8.52	0.66
Tree	GBR	6.17	0.67	4.81	0.85
	RF	6.67	0.67	3.88	0.89
	ETR	5.76	0.70	4.53	0.89

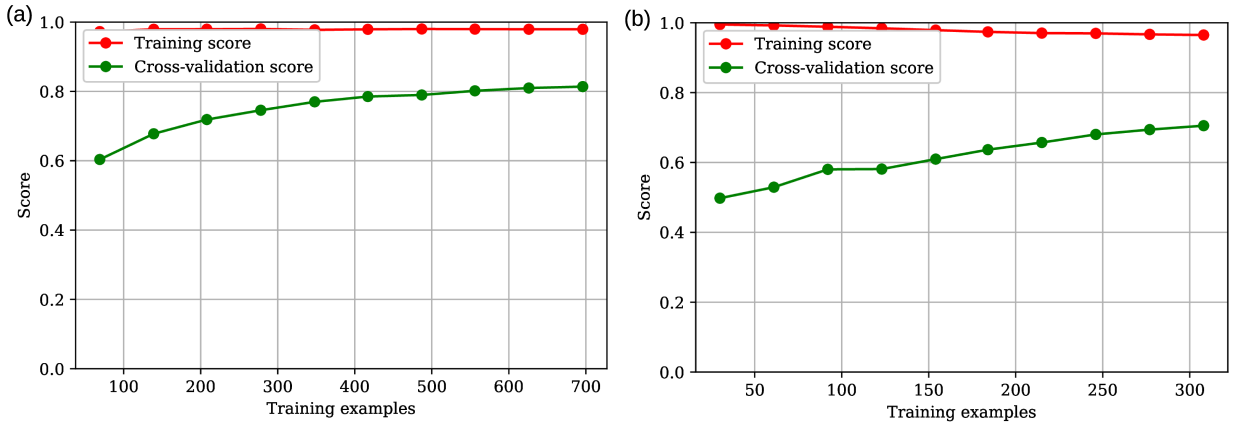

FIG. 2. Learning curve for (a) HYST and (b) THOR.

Learning curve of final selected models HYST and THOR are shown in Figure 2(a) and (b), respectively. The learning curves represent the performance of the models on a training set and a test set as a function of the number of training examples used. The x-axis represents the number of training examples, while the y-axis represents R2 score.

The feature ranking for final selected features in descending order of importance for HYST and THOR identified by the models averaged over 100 trials are shown in Figure 3 and Figure 4, respectively.

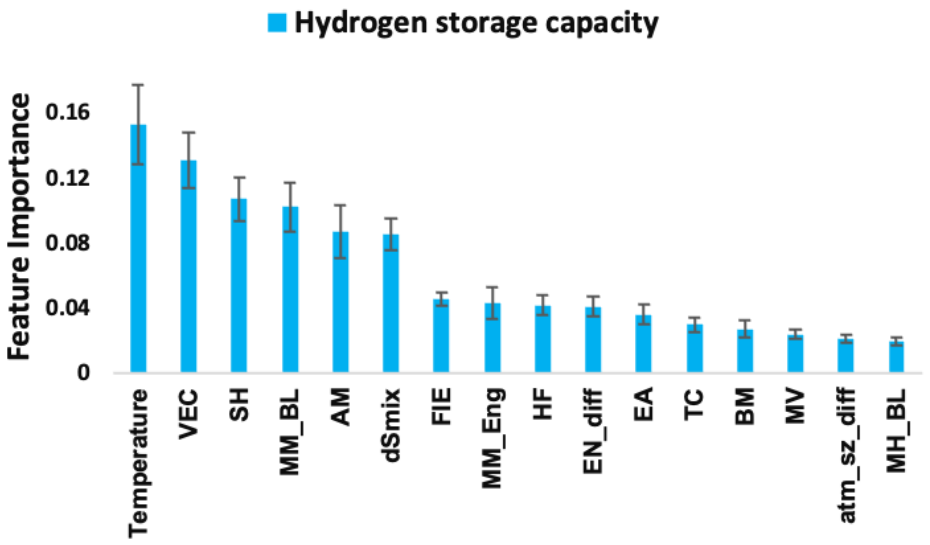

FIG. 3. Feature ranking plot in descending order of importance by the ETR model averaged over 100 trials for H2wt%.

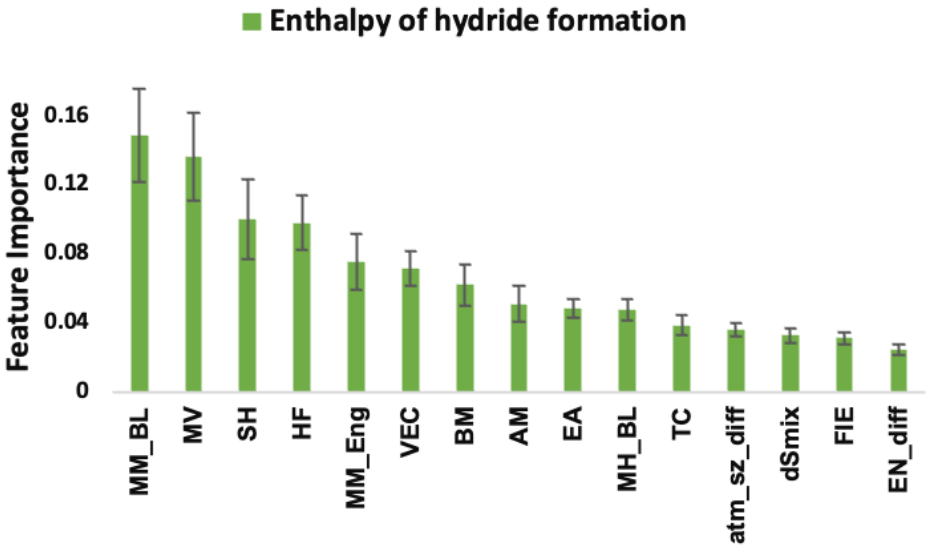

FIG. 4. Feature ranking plot in descending order of importance by the ETR model averaged over 100 trials for ΔH.

III. EFFECT OF ADDITION OF DATA ON HYST GENERALIZATION

Figure 5 illustrates the training and testing performance of a H2wt% model using dataset consisting of 857 data points. It is observed from the Figure 5(a) that a greater number of outliers are present in regions with higher weight percentages (circled data). This suggests

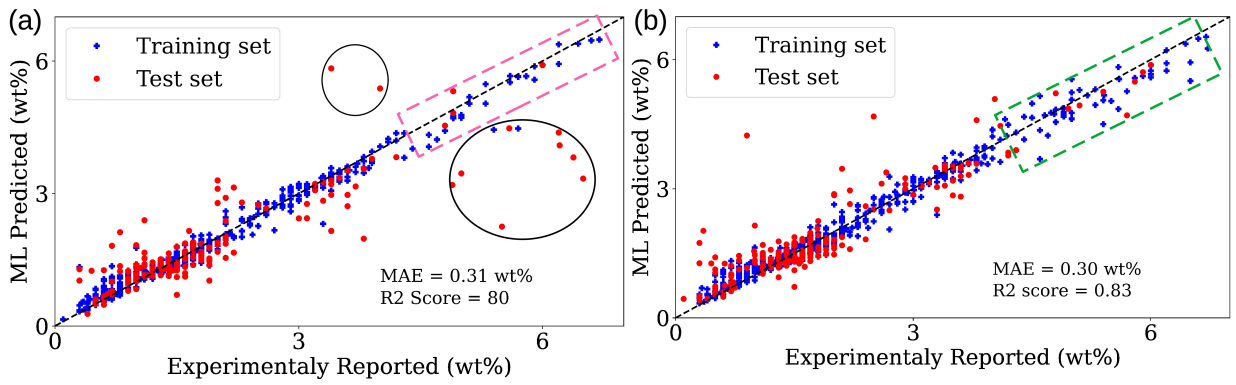

FIG. 5. ML predicted versus Experimentally reported train and test plot of H2wt% (a) with 857 data point and (b) 962 data point. No of outliers (circled data) reduces with addition of more data in higher weight percentage region (region highlighted with pink and green color rectangles.)

that the model's performance is suboptimal for compositions with higher hydrogen storage capacity. Subsequently, we curated data from literature and appended it to the original dataset, resulting in a new database consisting of 962 data points. The newly added data points predominantly comprised compositions whose experimental weight percentages were recorded in the higher weight percentage ranges. As anticipated, the model exhibited an improved performance, with lower number of outliers in higher weight percentage ranges, as well as an improved R2 score, as depicted in Figure 5(b).

IV. TRENDS OBSERVED IN PREDICTED HYDROGEN STORAGE PROPERTIES

The section discusses the changes observed when lithium (Li), titanium (Ti), and vanadium (V) are alloyed with the other 37 elements. The changes are illustrated in Figure 6, Figure 7 and Figure 8, respectively.

Figure 6 (a) shows the systematic change in Li based alloys hydrogen storage capacity (H2wt%) at room temperature with the addition of elements from different series. It is observed that alloying Li with other small hydriding elements such as magnesium (Mg), calcium (Ca), and aluminum (Al) results in improved weight percentage (wt%), although the enthalpy of hydride formation increases, making hydrogen desorption difficult at lower temperatures. Moreover, alloying Li with small fractions of transition metals such as zinc

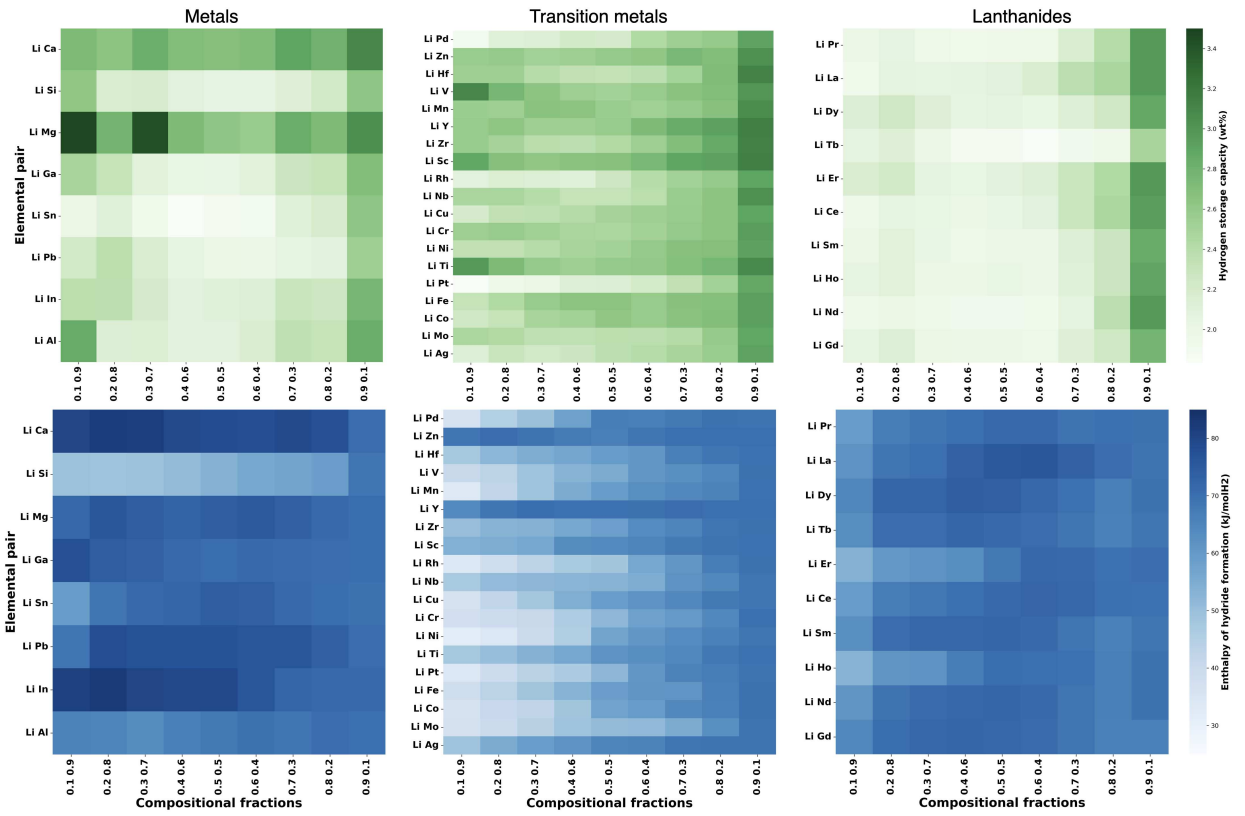

FIG. 6. Heat map representing (a) H2wt% and (b) ΔH of Li-based alloys when mixed with metals, transition metals and lanthanides.

(Zn), vanadium (V), yttrium (Y), scandium (Sc), titanium (Ti), and iron (Fe) leads to relatively higher H2wt% (> 3 wt%). Figure 6(b) represents the change in enthalpy of hydride formation (ΔH) for Li based alloys. It shows that alloying Li with other hydriding elements leads to the formation of stable hydrides. However, with an increasing concentration of certain elements such as silicon (Si), manganese (Mn), niobium (Nb), chromium (Cr), nickel (Ni), iron (Fe), and molybdenum (Mo), there is a decrease in ΔH of Li based alloys.

Similarly, Figure 7 and Figure 8 show the changes in H2wt% at room temperature and ΔH of Ti and V when alloyed with different series of elements. Ti and V are early lightweight transition metals that posses high affinity towards hydrogen and hence can form hydrides even at room temperature.

As illustrated in Figures 7 and Figure 8 (a) (b), the V-Ti alloy is among the most promising family with a high weight capacity (3.5 wt%) even at room temperature, along with lower ΔH. In addition, alloying V and Ti with Mg, Al, and Sc also shows promising hydrogen storage properties. Interestingly, the mixing of Ti and V with lanthanides leads

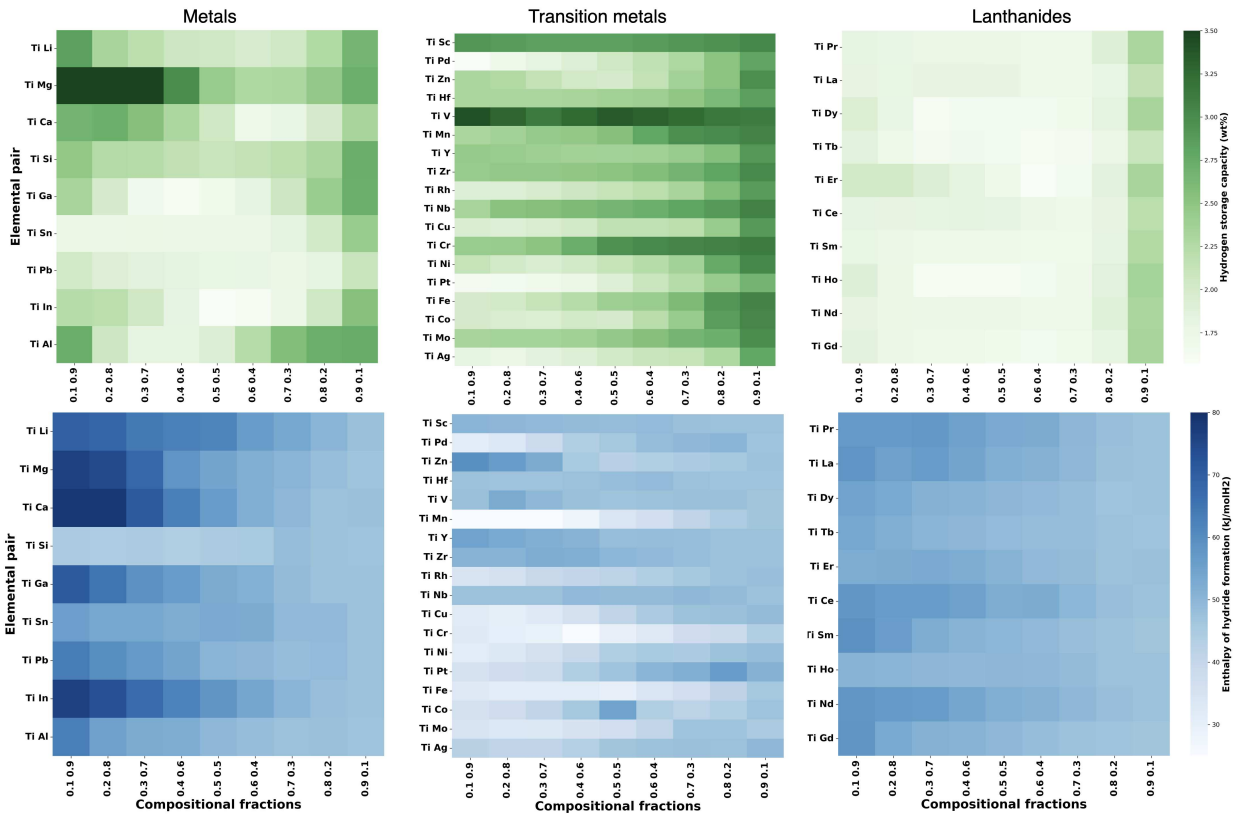

FIG. 7. Heat map representing (a) H2wt% and (b) ΔH of V-based alloys when mixed with metals, transition metals and lanthanides.

to the formation of unstable hydrides (lower ΔH), which suggests that a small fraction of these lanthanides in the promising families of V and Ti can further enhance their kinetics and thermodynamic properties.

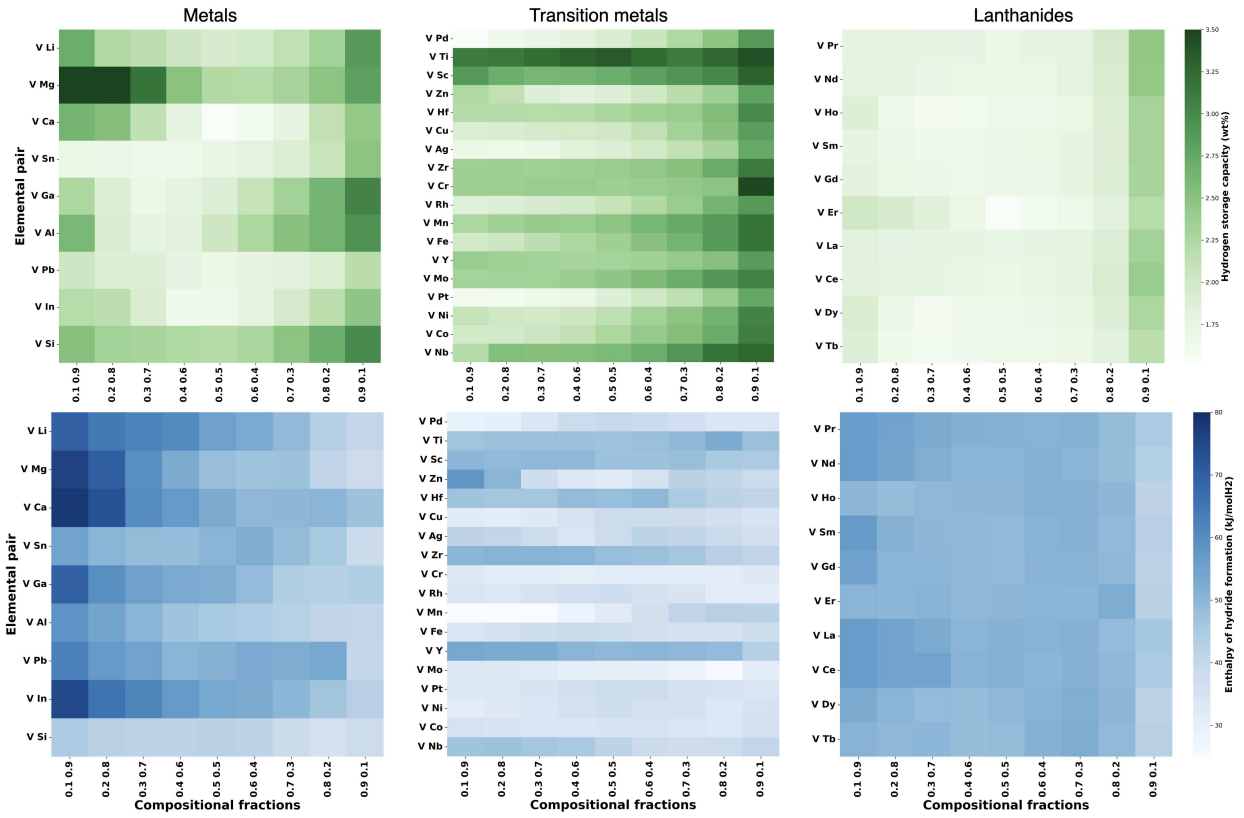

FIG. 8. Heat map representing (a) H2wt% and (b) ΔH of V-based alloys when mixed with metals, transition metals and lanthanides.